The Journal of Experimental Biology 213,673-682

doi:10.1242/jeb.035550

Venom kinematics during prey capture in *Conus*: the biomechanics of a rapid injection system

S. Michael Salisbury[1], Gary G. Martin[1], William M. Kier[2] and Joseph R. Schulz[1,*]

[1]Occidental College, 1600 Campus Road M-3, Los Angeles, CA 90041-3314, USA and [2]Department of Biology, University of North Carolina at Chapel Hill, Chapel Hill, NC 27599, USA

*Author for correspondence (jschulz@oxy.edu)

Accepted 24 November 2009

SUMMARY

Cone snails use an extensile, tubular proboscis as a conduit to deliver a potent cocktail of bioactive venom peptides into their prey. Previous studies have focused mainly on understanding the venom's role in prey capture but successful prey capture requires both rapid physiological and biomechanical mechanisms. *Conus catus*, a fish-hunting species, uses a high-speed hydraulic mechanism to inject its hollow, spear-like radular tooth into prey. We take an integrated approach to investigating the biomechanics of this process by coupling kinematic studies with morphological analyses. Taking advantage of the opaque venom and translucent proboscis of a mollusc-hunting juvenile cone snail, *Conus pennaceus*, we have determined that a high-speed prey capture mechanism is not unique to cone species that hunt fish prey. Two morphological structures were found to play crucial roles in this process. A constriction of the lumen near the tip of the proboscis, composed of tall epithelial cells densely packed with microfilaments, impedes forward movement of the radular tooth prior to its propulsion. Proximal to the constriction, a muscular sphincter was found to regulate venom flow and pressurization in the proboscis. In *C. pennaceus*, the rapid appearance and flushing of venom within the proboscis during prey capture suggests a mechanism involving the delivery of a discrete quantity of venom. The interplay between these elements provides a unique and effective biomechanical injection system for the fast-acting cone snail venom peptides.

Supplementary material available online at http://jeb.biologists.org/cgi/content/full/213/5/673/DC1

Key words: venom kinematics, biomechanics, functional morphology, prey capture, *Conus*.

INTRODUCTION

The genus *Conus* includes over 500 species of venomous predatory marine gastropods. During the last 50 million years cone snails have evolved into three general feeding groups based on prey preference: fish-hunters, worm-hunters and mollusc-hunters (Duda et al., 2001). The remarkable degree of diversification of the genus (Kohn, 1990) may be linked to the evolution of a novel high-speed prey capture mechanism. Cones utilize a long, flexible, hydrostatically-supported appendage, the proboscis, to sense and locate prey (Greene and Kohn, 1989). The proboscis subsequently functions as a conduit to deliver immobilizing venom, whose composition can vary both inter- and intraspecifically (Duda and Palumbi, 2000; Jakubowski et al., 2005; Davis et al., 2009). To envenomate prey, cone snails inject a harpoon-like radular tooth into their prey, allowing toxins to be delivered through the hollow central canal of the tooth (Kohn, 1956).

Previous studies have focused mainly on deciphering the molecular targets of individual venom peptides. The majority of these neuroactive peptides modulate the activity of voltage- and ligand-gated ion channels (Olivera, 1997; Olivera, 2001; Olivera, 2006). Other studies have demonstrated how positive selection may operate to enrich the diversity of venom peptides effective against a particular prey type (Duda and Palumbi, 1999; Duda, 2008; Remigio and Duda, 2008). Maintaining venom compositions that are effective on the physiology of distinct prey types is an essential aspect of prey capture in these slow-moving animals.

Successful prey capture requires both rapid physiological and biomechanical mechanisms. At least one fish-hunting species, *Conus catus*, uses a high-speed hydraulic mechanism. During this process the highly specialized radular tooth is fired from its holding point near the tip of the proboscis into the prey in less than 1 ms (Schulz et al., 2004). Prior to tooth ejection, a priming step occurs during which the radular tooth is forced against a constriction of the proboscis lumen. This constriction was thought to be a muscular sphincter (Greene and Kohn, 1989) that contracts to retain the radular tooth prior to its release (Schulz et al., 2004). The energy needed to propel the tooth was hypothesized to be generated by an increase in pressure caused by sustained contraction of the proboscis' musculature, eventually sending the tooth past the constriction and into the prey (Schulz et al., 2004). Although the rapid motion of the radular tooth has been established, the mechanism responsible for generating this motion remains unclear.

The present study takes an integrated approach to investigating the biomechanics of high-speed prey capture by coupling kinematic studies with morphological analyses. To directly visualize venom dynamics during *Conus* prey capture we took advantage of the opaque venom and translucent proboscis of a mollusc-hunting juvenile cone snail, *Conus pennaceus*, to record kinematics with high-speed video. Using light, fluorescence and transmission electron microscopy (TEM), we assessed the composition and function of specific tissues crucial for prey capture. Our integrative experimental approach offers a more comprehensive understanding of this well-developed mechanism in *Conus*.

Kinematic studies of the mollusc-hunting *C. pennaceus* indicate that a high-speed prey capture mechanism is not unique to cone species that hunt fish prey capable of rapid escape responses. *Conus pennaceus*

also hydraulically propels a radular tooth past a constriction of the proboscis lumen. This constriction is not a muscular sphincter. Instead, it is composed of tall epithelial cells containing an array of intracellular microfilaments. A dense muscular sphincter is present midway along the extended proboscis. Proximal to the muscular sphincter, an increase in tortuosity, or kinking, of the lumen well in advance of the appearance of venom in the proboscis suggests that the muscular sphincter actively regulates venom dynamics within the proboscis. Tooth movement coincided with the sudden appearance of venom flowing within the lumen. The interplay between these elements provides a novel and effective biomechanical injection system for fast-acting venom peptides found in *Conus*.

MATERIALS AND METHODS

Experimental animals

Adult specimens of *Conus catus* (Hwass 1792; 2–4 cm shell length) and juvenile *Conus pennaceus* (Born 1778; <2.3 cm) were collected from Kauai, HI, USA. Animals were maintained in separate 10 gallon (37.85 l) saltwater tanks at Occidental College, Los Angeles, CA, USA. *Conus catus* were fed freshly killed *Fundulus parvipinnis* and *Clevelandia ios*. *Conus pennaceus* was fed live *Nassarius* species (<1 cm) and *Strombus maculates* (<1 cm).

Histology

For histological analysis, elongated proboscides of *C. catus* (<2 cm) were severed from the snail immediately prior to a prey capture. Although snails later regenerated a fully functional proboscis, regenerated proboscides were not used for morphological studies. The proboscis was sectioned in sagittal (parallel to the longitudinal axis and dorsoventrally aligned), longitudinal (parallel to the longitudinal axis) and transverse (perpendicular to the longitudinal axis) orientations. For both light microscopy and TEM, proboscis tissue was fixed overnight in 2.5% glutaraldehyde in 0.1 mol l^{-1} sodium cacodylate, pH 8.1, containing 12% glucose. Tissues were rinsed in 0.1 mol l^{-1} sodium cacodylate, postfixed for 1 h in 1% OsO_4 in 0.1 mol l^{-1} sodium cacodylate and stained for 1 h in 3% uranyl acetate in 0.1 mol l^{-1} sodium acetate. After dehydrating in a graded ethanol series, tissue was infiltrated overnight and embedded in Spurr's (Spurr, 1969) resin at 70°C. Thick sections (0.5–1.5 μm), from a minimum of three animals, were stained with Methylene Blue (2.5% Methylene Blue, 2.5% borax in water) and examined with light microscopy. Thin sections (50–70 nm) were cut with an NOVA ultramicrotome (LKB, Sweden) and spread with xylene vapor. The sections were stained for 5 min in lead citrate (boiled aqueous solution) and examined by TEM (Zeiss EM 109, Oberkochen, Baden-Wurttemberg, Germany). Images obtained were analyzed using Image J software (Rasband, W.S., ImageJ, U.S. National Institutes of Health, Bethesda, MD, USA, http://rsb.info.nih.gov/ij/, 1997–2008). Sample sizes for morphometric analyses for both light microscopy and TEM were at least N=15 (unless otherwise noted). Measurements were selected at random within the region of interest. To quantify the density of fibers 40 μm areas were sampled at random, and 1 μm areas were an analyzed for the presence of filaments. Statistical significance was determined using Student's t-tests.

Fluorescent labeling

Cellular filamentous actin (f-actin) networks were identified with rhodamine-phalloidin (Invitrogen, Carlsbad, CA, USA). *Conus catus* (<3.5 cm, N=3) proboscides were obtained in the same manner as described above and fixed overnight in 4.5% paraformaldehyde in phosphate buffered saline (PBS), pH 7.6. Proboscis tissue was embedded in 5% low-melting point agarose in PBS prior to hardening. Sections (30–50 μm) were cut with a vibrating microtome (Model 1000, The Vibratome Company, St Louis, MO, USA). The sections were washed with PBS and treated with 1% Nonidet P-40 for 10 min to permeabilize cellular membranes, then washed in PBS again. Bovine Serum Albumin (1%) in PBS was used as a blocking agent. Sections were stained for 1 h in a 1:60 dilution of a rhodamine-phalloidin stock solution. Immediately following labeling, sections were washed three times in PBS for 5, 15 and 60 min, respectively. Labeled sections were mounted on glass slides with Vectashield (Vector Laboratories, Burlingame, CA, USA) anti-fade medium containing DAPI and sealed with clear nail polish (Wollensen et al., 2007). f-actin was observed using epifluorescence microscopy on a Nikon E800 microscope (Nikon, Tokyo, Japan) and the resulting images color combined with Metamorph™ software (Molecular Devices, Sunnyvale, CA, USA). Images were further adjusted for brightness and contrast using Photoshop 7.0 (Adobe Systems, Mountain View, CA, USA).

High-speed video recordings

Prey-capture events of *C. pennaceus* were recorded using high-speed video. A color high-speed camera (Pixelink, PL-A742, Ottawa, ON, Canada) operating at 325 frames per second (frames s^{-1}) was mounted above a custom acrylic viewing chamber. A juvenile *C. pennaceus* was coaxed to extend its proboscis down a recording channel (1.9 mm × 20 mm × 1.7 mm) by placing prey at the other end [apparatus similar to that described in Schulz et al. (Schulz et al., 2004)]. For improved optical quality, a glass slide was placed over the top of the trough. Six 150 W fiber optic light beams provided sufficient light to the chamber during filming. The actual frame rate of the high-speed camera was confirmed using a PowerLab (AD Instruments, Colorado Springs, CO, USA) to trigger paired strobe discharges at various intervals. By capturing the flashes with the camera and counting the frames in the intervals we were able to directly confirm the camera's frame rate.

Video analysis

Sequential still frames from eight individual *C. pennaceus* prey capture events were compiled using Photoshop 7.0 and analyzed with Image J. The analyses consisted of measuring proboscis lumenal deflection, lumen expansion and gray-scale values to monitor venom dynamics. Deflection of the lumen was quantified by measuring the distance from the midline of the proboscis to the middle of the proboscis lumen. Measurements were made approximately 1.3 mm proximal to the muscular sphincter. Values obtained were normalized. To determine time constants for the rate of pressurization within the proboscis, traces were fitted with single exponentials in Igor Pro® (Wavemetrics, Inc., Lake Oswego, OR, USA) and those values were averaged within the respective populations of data. To quantify venom dynamics in the proboscis, gray-scale measurements of a 170 μm × 125 μm box were made both proximally and distally to the muscular sphincter (2.6 mm apart). Changes in gray-scale values were correlated to the change in venom density. Data were normalized and expressed as a power function. For display purposes the lowest and highest mean values were set to 0 and 1, respectively. To analyze the expansion of the lumen wall, the diameter of the lumen was measured (from circular musculature on opposite sides of the lumen) at the time points shown. Statistical significance was determined using a Student's t-test.

3-D reconstruction

Computer-assisted 3-D reconstruction was used to visualize the details of the circum-lumenal muscular sphincter. Longitudinal thick

sections (1 μm) of approximately half of the muscular sphincter were photographed (every 8 μm) and aligned using a visualized best-fit method with ImageReady 7.0 (Adobe Systems). Aligned images were uploaded into the *Reconstruct*: 3-D remodeling program (Fiala, 2005), and outlines of tissues were traced using a graphics tablet. The program rendered a 3-D reconstruction that could be visualized in any orientation.

RESULTS

Functional morphology of the constriction

Sections of the anterior tip of *C. catus* proboscides reveal a constriction of the lumen wall located approximately 2 mm from the elongated tip, previously noted during videography of high-speed prey capture (Schulz et al., 2004). The lumen wall, defined as the lumenal epithelium and its surrounding musculature, provides the conduit for venom flow during prey capture. The constriction is a 300 μm-long portion of the lumen wall with a reduced internal lumen diameter (Fig. 1A,B). When viewed in transverse section the constriction has an arch-like symmetry; the epithelium of the dorsal and both lateral sides is thickened, reducing the internal lumen diameter (Fig. 1A). The functional significance of this asymmetry is unclear. The constriction is composed of columnar epithelial cells (79±0.9 μm in height) protruding into the lumen. The cytoplasm in these cells stains homogeneously with Methylene Blue (Fig. 1D). Distal to the constriction epithelial cells are shorter (60±0.4 μm) with a similar staining pattern (Fig. 1E). The epithelial cells proximal to the constriction are taller (116±1 μm) and are composed of a largely clear cytoplasm with folded ribbon-like structures dispersed throughout the cytoplasm (Fig. 1C). The presence of different cytoplasmic elements in the proximal cells suggests a distinct function as compared with those of the epithelium in the region of the constriction.

Ultrastructural analysis reveals significant differences in microfilament distribution within the cytoplasm of the lumenal epithelium. An electron-dense meshwork of microfilaments exists throughout the cytoplasm of the epithelium from both the region of the constriction (Fig. 2A,C) as well as the distal region (data not shown). This meshwork shows a preferred orientation in the radial direction and consists of microfilaments 3.1±0.3 nm in diameter. In longitudinal sections of the proboscis, a 200 nm electron-lucent area is present between the microfilaments and the plasma membrane in the region of the constriction (Fig. 2C), suggesting the microfilaments are not anchored to the plasma membrane. In marked contrast, the epithelial cells in the proximal portion have an electron-lucent cytoplasm with folded sheets of electron-dense microfilaments (Fig. 2B,D). The folded structures appear to be concentrated near the nuclear membrane and extend as strands throughout the cytoplasm. The diameter of these filaments (3.7±0.3 nm) was not significantly different from those of the other epithelial cells analyzed (P>0.05).

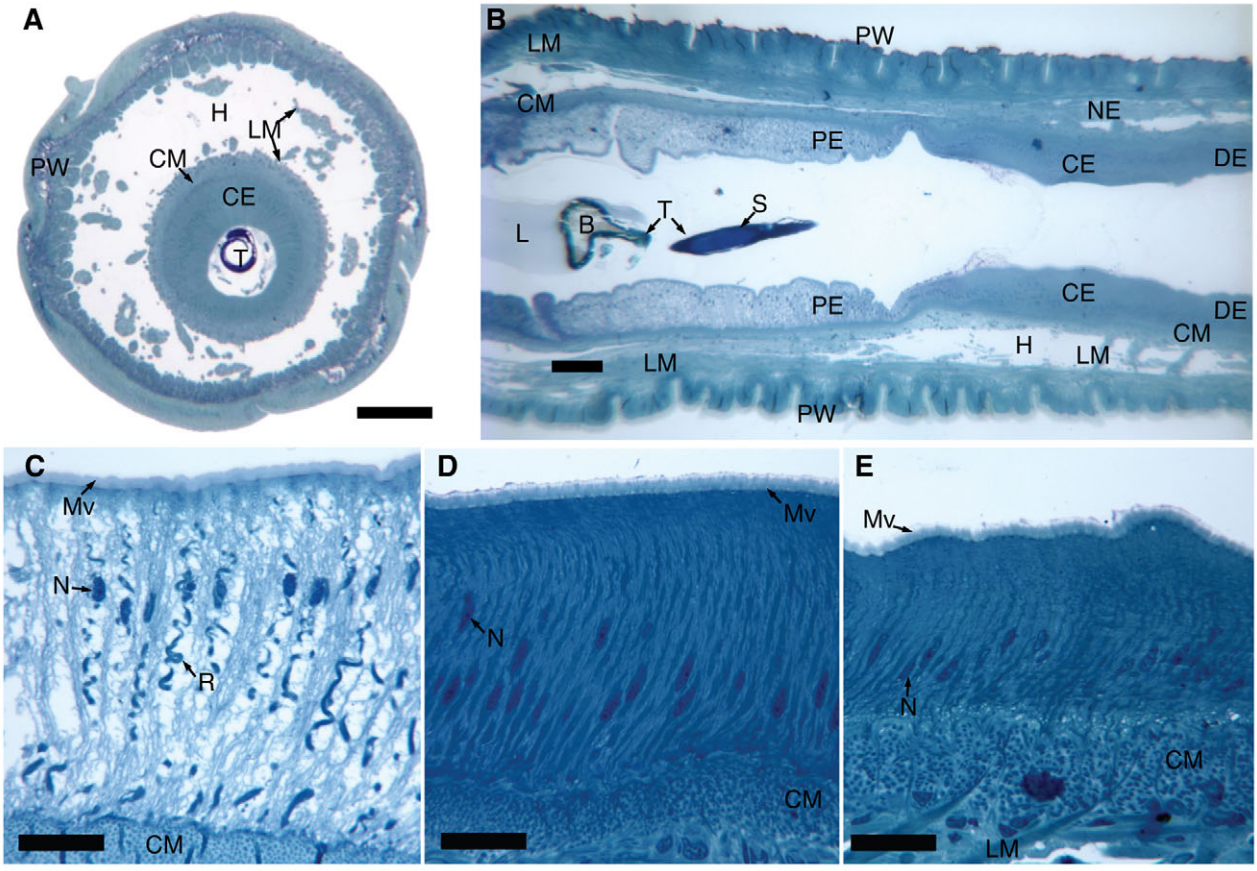

Fig. 1. Light micrographs of *Conus catus* proboscis sections stained with Methylene Blue. (A) Transverse section of the proboscis at the constriction (dorsal surface oriented up). (B) Longitudinal section of the constriction near the tip of the proboscis (distal to the right). High magnification views of the proximal (C), constrictional (D) and distal epithelial cells (E) (apical face up). Sections in A and B contain different amounts of hemocoel (H). Scale bars: A,B=100 μm; C–E=25 μm. B, bulbous base of radular tooth; CE, constrictional epithelium; CM, circular musculature; DE, distal epithelium; L, ligament; H, hemocoel; LM, longitudinal musculature; Mv, microvilli; N, nucleus; NE, nerve; PE, proximal epithelium; PW, outer proboscis wall; R, ribbon-like microfilaments; S, shaft of radular tooth; T, radular tooth.

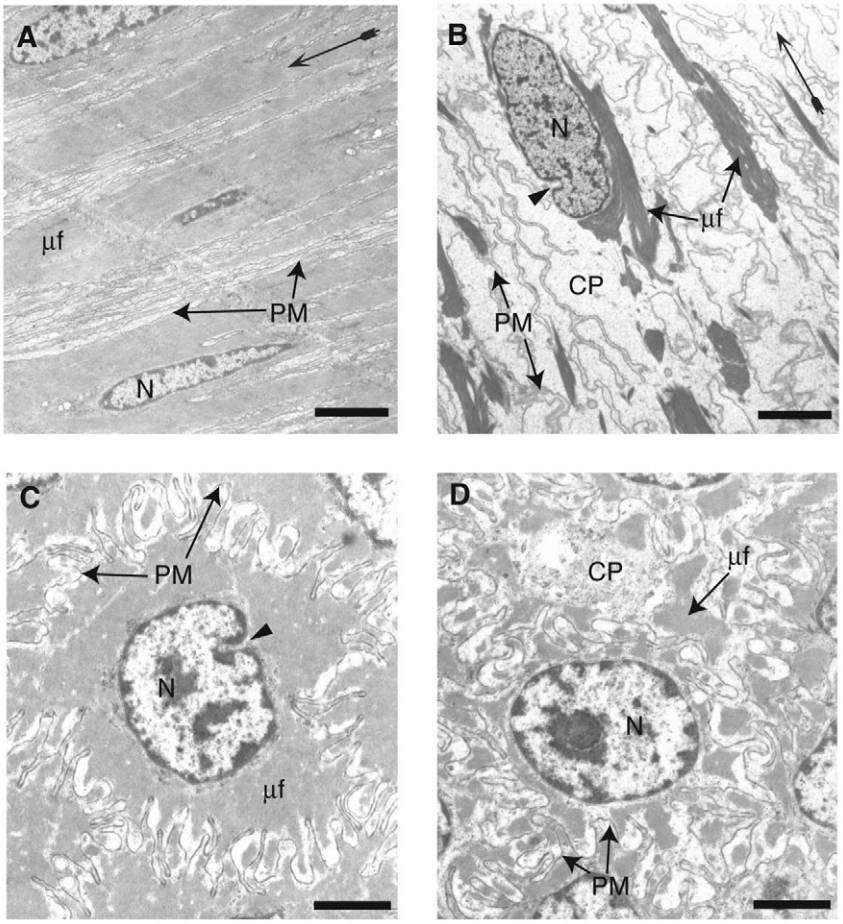

Fig. 2. Transmission electron micrographs of *Conus catus* proboscis lumen epithelial cells. Transverse sections of the proboscis showing cells in both the constrictional (A) and proximal (B) locations. Full arrows indicate direction towards the central lumen. Scale bars: A,B=4 μm. Longitudinal proboscis sections of both constrictional (C) and proximal (D) epithelia demonstrating the irregularity of microfilaments in proximal cells and the interdigitated plasma membranes in both cell types. Arrowheads demonstrate nuclear invaginations. Scale bars: C,D=2 μm. CP, cytoplasm; μf, microfilaments; N, nucleus; PM, plasma membrane.

Longitudinal sections of the lumenal epithelium revealed hexagonal cells with interdigitating folds of the plasma membranes. In addition, nuclei observed had invaginations of the nuclear envelope (Fig. 2B,C). Intermediate junctions are present in the folded plasma membrane near the apical face (S.M.S., unpublished) potentially preventing leakage of peptides from the lumen.

Phalloidin staining was performed to verify the molecular composition of the microfilaments. Labeling of the *f*-actin shows that the lumenal epithelia is attached basally to intensely staining circular and longitudinal smooth muscle (Fig. 3A). The dorsal and ventral epithelia, although containing structural differences, have similar *f*-actin distributions within the cells (Fig. 3A). The apical surface of the epithelia showed an increased phalloidin staining, presumably due to the terminal actin webs underlying the microvilli. Higher magnification demonstrates radially oriented fibers in the cytoplasm of the constrictional and distal epithelium (Fig. 3B, second and third columns). The ovate nuclei in the constrictional and distal epithelial cells, stained with DAPI, are located approximately equidistant from the basal lamina. This organization of cells could provide additional support to the lining of the lumen. In the proximal cells, the epithelium appears to have actin filaments attached to infoldings of the lumen wall (Fig. 3B, first column). The filaments begin as a dense bundle and branch as they extend to reach the apical face of the epithelium. The radiating pattern of the nuclei parallels the arrangement of the fibers. This difference in pattern of cytoplasmic *f*-actin networks within the epithelia was thus observed in both light and electron microscopy.

Venom kinematics during prey capture

During *C. pennaceus* prey capture, a radular tooth is hydraulically propelled into the flesh of its prey. Analysis of high-speed video sequences (e.g. supplementary material Movie 1) shows that as the snail extends its proboscis; the tip of the 2 mm-long spear-like tooth sits approximately 700 μm from the tip of the proboscis (Fig. 4A, panel a). This distance allows for acceleration of the radular tooth before impalement of the prey. The bulbous base of the radular tooth (Fig. 1B) is pushed forward 200 μm during a priming phase within the last 3 ms prior to its release (supplementary material Fig. S1), and is forced up against the constriction of the lumen within the proboscis (Fig. 4A, panel c). This observation provides a possible biomechanical context for the dense intracellular scaffolding within the epithelium in the constricted portion of the proboscis of *C. catus* (Fig. 1B,D and Fig. 3A). Initial movement suggests growing pressure behind the tooth. Within 3 ms the base of the disposable tooth is ejected 1.5 mm past the constriction, propelling it to the tip of the proboscis (supplementary material Fig. S1), which implies a minimum velocity of 0.66 m s^{-1}. After ejection, the base of the tooth is prevented from leaving the proboscis by a band of circular muscles at the proboscis tip (supplementary material Fig. S2) while venom flows through the tooth central canal and is injected into the prey. The bands of circular muscle at the tip provide an effective way to retain the base of the tooth during venom injection.

Prior to tooth ejection, *C. pennaceus* begins an elaborate pressurization process that is responsible both for firing the tooth and injecting the venom (Fig. 4B). Before the priming step, a rapid increase in tortuosity, or kinking, of the lumen wall occurs proximal to a muscular sphincter, suggesting an increase in pressure is occurring

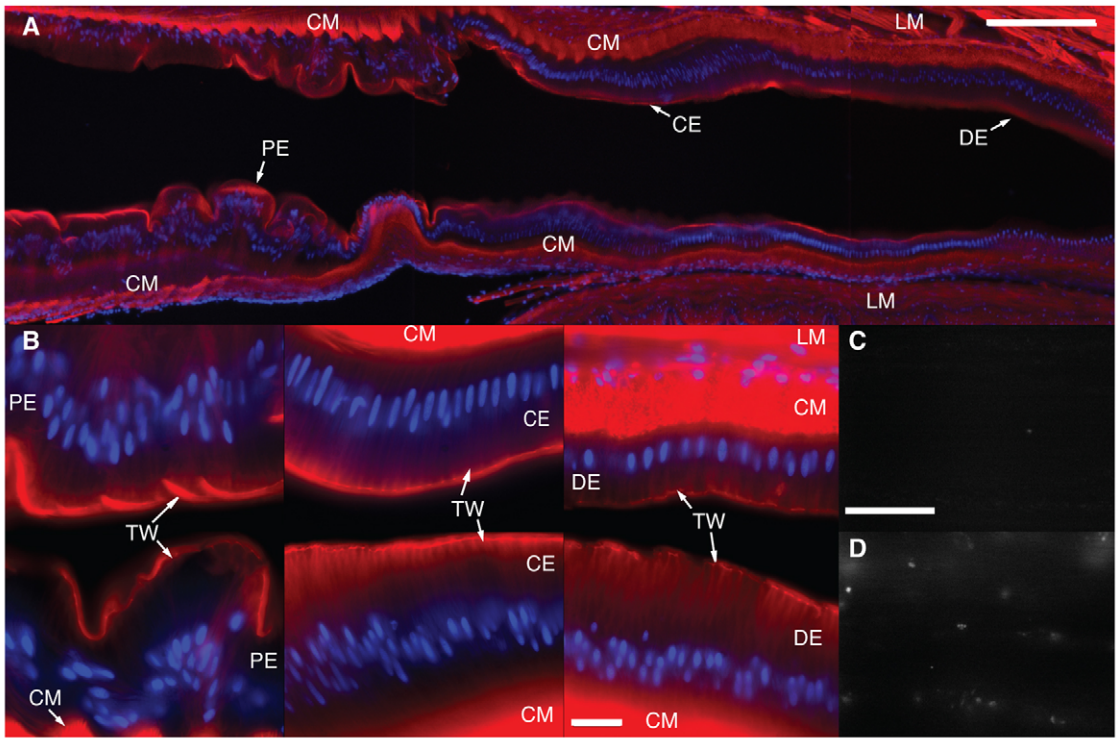

Fig. 3. Fluorescent images of the constrictional and adjacent epithelia from *Conus catus* showing the labeling of *f*-actin with rhodamine-phalloidin (red) and nuclei with DAPI (blue). Photo-composite sagittal section of the constrictional region (A) and control unlabeled section (C). Oriented with dorsal up and the distal tip of the proboscis to the right. Scale bar=200 μm. (B) Higher magnification views of the proximal (first column), constrictional (second column) and distal (third column) epithelium. (D) Control unlabeled image for the higher magnification view. Scale bars: 25 μm. CE, constrictional epithelium; CM, circular musculature; DE, distal epithelium; LM, longitudinal musculature; PE, proximal epithelium; TW, terminal web.

in that region of lumen (Fig. 4A, panel b arrows). During this process the lumen maintains its translucency, indicating that the venom, which contains opaque granules, is not present. Two distinct timings of this behavior were observed, commencing at either 200 ms or 120 ms before tooth ejection [Fig. 4B (1a and 1b) Fig. 5C]. Although *C. pennaceus* often injected its prey twice, no behavioral observations could be correlated to the two distinct timings. Rising phases of both populations of data were fit with single exponentials, and had similar time constants (200 ms: =10.83 ms; 120 ms: =10.96 ms; $P>0.05$).

Venom flow through the proboscis lumen coincides with the initiation of the priming step and hydraulic propulsion. Appearance of the venom in the lumen occurs suddenly 12 ms before tooth injection (Fig. 4A, panel c). Density measurements show venom entering the lumen and passing through a sphincter surrounding the proboscis lumen (Fig. 5A). Venom density increases at a rapid linear rate both prior to and immediately following release of the tooth (at 0 ms; Fig. 5B), increasing at similar rates and without delay both proximal and distal to the muscular sphincter (Fig. 5B). At 10 ms after propulsion of the radular tooth, the density of venom saturates and then declines (Fig. 5A) as it is forced through the hollow cavity of the radular tooth (Fig. 4A, panels e and f). Comparison of venom density proximal and distal to the muscular sphincter at each respective time point showed no significant differences ($P>0.05$), indicating that venom is not transiently stored by expansion of the proximal lumen but flows immediately through the dilated muscular sphincter. Venom appears to be expelled from the proboscis within 150 ms (Fig. 5A) followed by subsequent retraction of the proboscis approximately 200 ms after tooth injection (Fig. 4A, panel f), either leaving the radular tooth behind in the prey or retaining the tooth by its bulbous base (as in supplementary material Movie 1).

High-speed video shows the venom flow as a focused stream after passing through the sphincter. Close examination of *C. catus* high-speed video microscopy (Schulz et al., 2004) reveals that the translucent proximal epithelial cells fill the lumen cavity behind the base of the tooth prior to the priming step (morphology shown here in Fig. 1C). During the priming step, a jet of venom streams through the sphincter into the lumen compressing the proximal epithelium (Fig. 4A, panel c). This incursion of fluid causes the initial tooth movement of the priming step and may serve to store elastic energy in the walls of the lumen. For both *C. pennaceus* (Fig. 5D) and *C. catus* (supplementary material Fig. S3) the drastic increase in fluid volume causes expansion of the lumen directly behind the base of the tooth. Venom flow appears to retain its linear trajectory, suggesting initial expansion is due to displacement of the lumenal fluid (Fig. 4A, panel c). In *C. pennaceus* the lumen's diameter swells by 40% just 3 ms prior to release of the tooth. By filming at a higher frame rate, *C. catus*' lumen expansion was measured to peak just 2 ms (35% expansion) prior to hydraulic propulsion of the tooth. In both species, the lumen wall recoils rapidly following maximal expansion. Simultaneously, the tooth is forced against the constriction of the lumen wall, before it is discharged for impalement (Fig. 4, panel d).

Functional morphology of the circum-lumenal muscular sphincter

In all *Conus* species examined, a muscular sphincter is situated midway along the extended proboscis. Partial 3-D reconstruction of the sphincter demonstrates that it symmetrically encircles the lumen wall (Fig. 6). Nerve bundles oriented parallel to the lumen diverge away from the sphincter, suggesting that smaller fibers innervate it

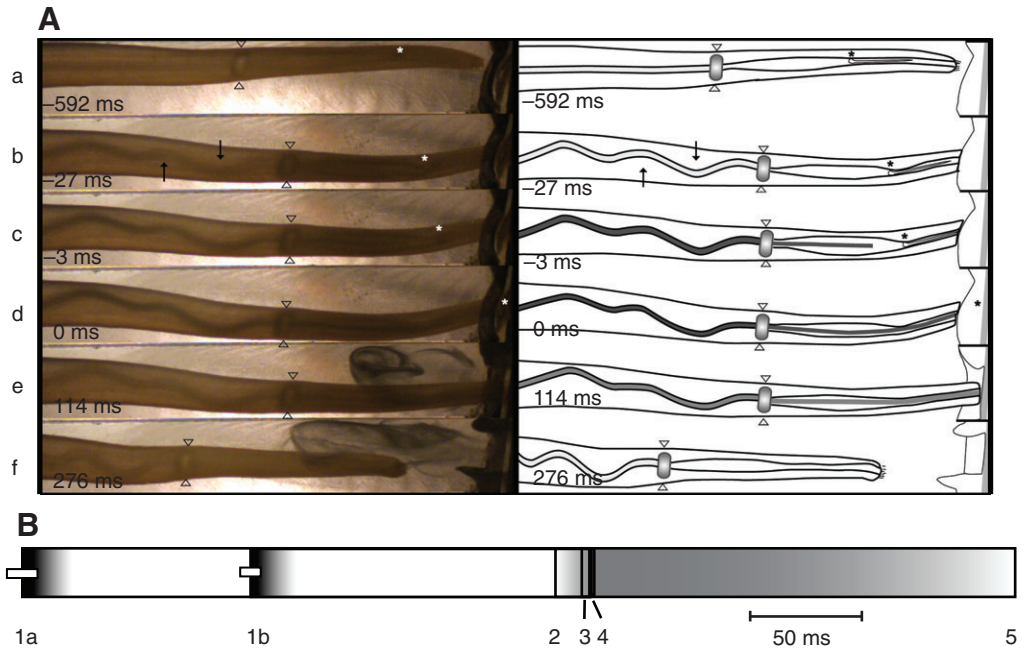

Fig. 4. Mechanism of prey capture in *Conus pennaceus*. Images of *Conus pennaceus* extending its proboscis towards the prey (a snail) in a recording channel. (A) Left column: sequential still frames taken from high-speed video (325 frames s^{-1}) illustrating venom movement through the central lumen of the proboscis. Right column: diagrams illustrating venom movement through the proboscis lumen at various densities (light gray=less dense, dark gray=more dense) passing through the muscular sphincter. 0 ms indicates the frame immediately following radular tooth propulsion. Arrowheads indicate the location of the muscular sphincter. Asterisks mark the position of the base of the radular tooth. Arrows indicate the initial increase in lumenal kinking. (B) A timeline showing the time scale of different processes during prey capture (to scale). Pressurization of the lumen occurs rapidly (1a or 1b, shading, dark to light, represents time course) before venom density begins to rise (2, shading represents increase in venom density within the lumen). The priming step (3) occurs 3 ms before the hydraulic propulsion of the radular tooth (4). Venom density starts falling after tooth ejection (5). Horizontal bars represent s.e.m. of start times of lumenal deflection for 1a and 1b.

(Fig. 6A,B). The orientation and position of the sphincter suggests that it causes localized constriction of the lumen during contraction.

The muscular sphincter is a densely packed structure with muscle fibers arranged in a ring surrounding the proboscis lumen. Ultrastructural analysis reveals that this sphincter is composed of smooth muscle cells (SMCs; Fig. 7). Morphometric measurements of the muscular sphincter show that the mean number of fibers is 0.29±0.01 fibers μm^{-2} (N=10). Samples of the adjacent longitudinal muscle (supplementary material Fig. S4) showed fewer fibers per unit area (0.16±0.01 fibers μm^{-2}, N=10). The difference between the fiber densities in sphincter and longitudinal muscle was significant (P<0.005). Transverse sections of the muscular sphincter revealed elongate smooth muscle fibers running axially (Fig. 7D). This provides the necessary musculature for the sphincter to gate venom flow observed in the high-speed footage (Fig. 4A, panels b–d).

Two types of smooth muscle fibers were identified in the muscular sphincter of *C. catus*, based on measurements of thick filament size, thick filament density and approximate cell dimensions (measured at the cell's greatest diameter). One type of fiber (SMCa; Fig. 7A,B) is larger and includes thick filaments greater diameter. The thick filaments of this fiber type are 64±8 nm in diameter (supplementary material Table S1) and show an unusual degree of morphological heterogeneity in comparison with other SMCs within the proboscis. The functional significance of this variation is unclear. They also show a 2-fold lower thick filament density (41±3.6 filaments m^{-2}, N=5; P<0.005), compared with the other SMCs analyzed (supplementary material Table S1). Sarcoplasmic reticulum is localized within these fibers near the sarcolemma.

The other class of SMCs in the muscular sphincter has an electron-dense cytoplasm (SMCb; Fig. 7A,B). The thick filaments of these fibers have a mean diameter of 43±0.9 nm, significantly smaller than the other fiber type (P<0.05, N=6). The thick filament density in SMCb (85±5.6 filaments μm^{-2}, N=5) is similar to that of longitudinal muscle (92±6.9 filaments μm^{-2}, N=5) from the adjacent regions (supplementary materials Fig. S4 and Table S1; P>0.05). Higher thick filament density of SMCs is often correlated with greater peak muscle fiber tension during contraction (Plesch, 1977). SMCb's have smaller, compressed sarcoplasmic reticulum lining their plasma membranes compared with SMCa and longitudinal muscles. The thin filaments in both fiber types of the muscular sphincter were difficult to resolve with TEM. In all SMCs small finger-like invaginations of the membrane similar to those found in *Clione* (see Discussion) were observed (Huang and Satterlie, 1989).

DISCUSSION

Conus pennaceus, a snail-hunter, uses a high-speed hydraulic prey capture mechanism similar to the fish-hunting *C. catus*. We estimate that *C. pennaceus* propels its harpoon-like radular tooth at a velocity of 0.6 m s^{-1} (videography taken at 325 frames s^{-1}). The velocity is likely to be even higher as the frame rates of the video sequences in this study and the previous study on *C. catus* [1000 frames s^{-1} (Schulz et al., 2004)] were not high enough to resolve the peak velocity. Nonetheless, a high-speed mechanism has now been described in two species of *Conus* representing two of the three predatory groups. In addition, standard video (~30 frames s^{-1}) of prey capture by a worm-hunting snail, *Conus imperialis*, was too slow to resolve radular tooth movements, suggesting a similarly rapid mechanism in this group as well (Kohn and Hunter, 2001) (J.R.S. and S.M.S., unpublished). Even the ominivorous *C. californicus*, located basally in the genus (Duda

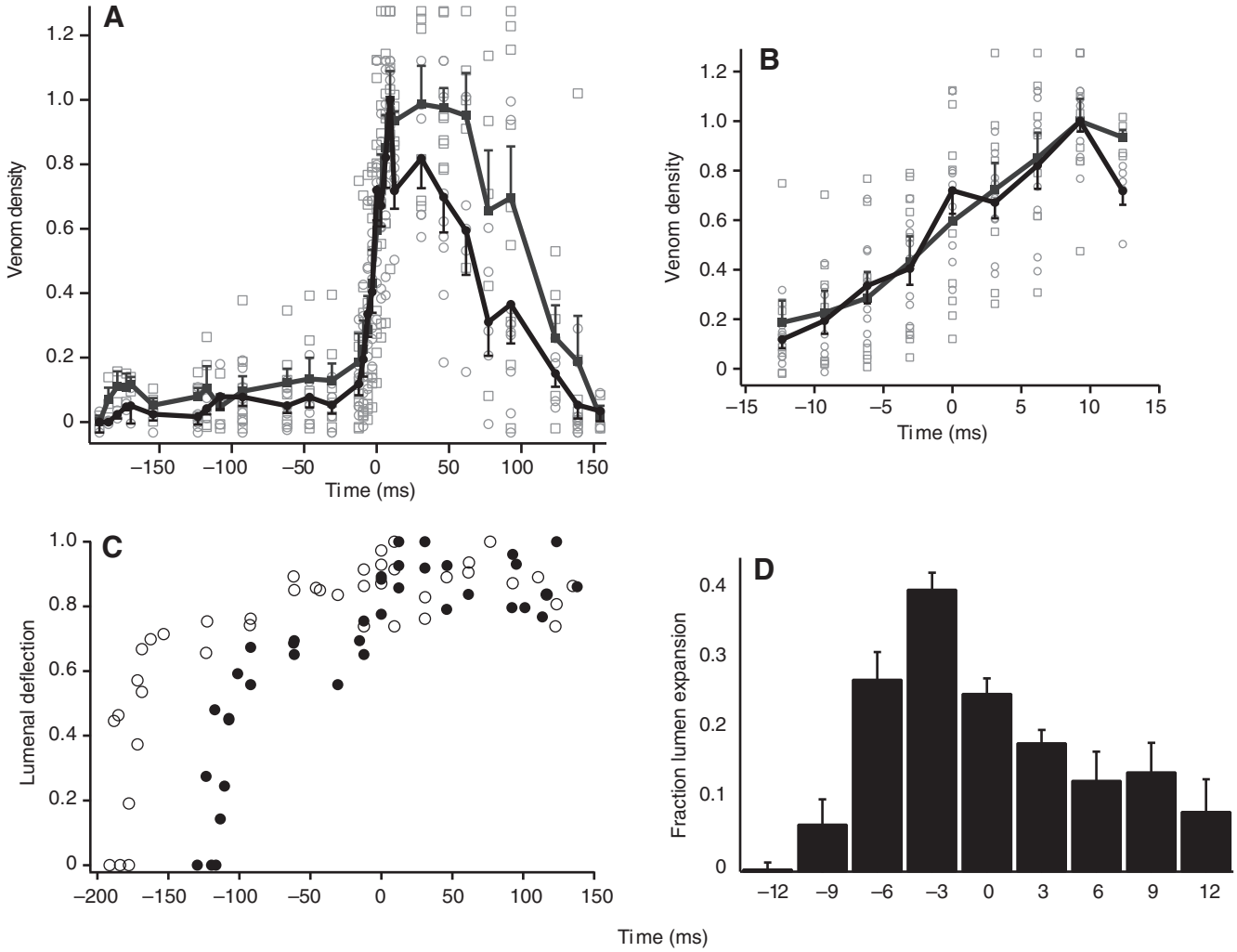

Fig. 5. Quantification of the kinematics of prey capture in *Conus pennaceus*. Plot of venom flow through the central lumen of the proboscis (A). Expanded time scale of data within 15 ms pre- and post-tooth ejection (B). Venom density plotted for values proximal (light-gray circles) and distal (light-gray squares) to the muscular sphincter. Mean values plotted as black circles and dark gray squares, respectively. Error bars=s.e.m. Measurement of the relative deflection of the lumen within the proboscis (C; *N*=8). Two distinct timings are indicated by open and filled circles. Expansion of the lumen wall behind the base of the radular tooth during prey capture (D). 0 ms indicates the frame immediately following radular tooth propulsion.

et al., 2001; Duda and Kohn, 2005), uses a prey capture mechanism too rapid to be resolved by standard video (Stewart and Gilly, 2005). These data suggest that the rapid hydraulic propulsion of a radular tooth is a genus-wide phenomenon used during prey capture.

The constriction of the lumen near the tip of the proboscis is integral to limiting radular tooth movement prior to its release during the priming step (supplementary material Fig. S1). This structure was originally thought to be a muscular sphincter that prevents the tooth from slipping backward during prey capture (Greene and Kohn, 1989). Schulz et al. demonstrated that the constriction prevents forward movement of the tooth prior to being injected into prey (Schulz et al., 2004). In the present study we have shown that this structure is not a muscular sphincter but is formed of a thickened epithelium supported intracellularly by a scaffold of *f*-actin (Fig. 3). The scaffold of microfilaments may provide the mechanical integrity that is required to resist forward progression of the radular tooth while venom is pressurizing behind it. The morphology (invagination of the nuclei and interdigitating plasma membranes) of these cells is similar to that of SMCs involved in hamster ovulation (Martin and Talbot, 1981). This is not surprising, as it has been noted that a cone snail can extend its proboscis greater than 15 times its contracted length in search of prey [approximately 1.5× shell length (Greene and Kohn, 1989)]. The extension of the proboscis requires a mechanism for accommodating the extreme strains experienced by epithelial cells. Actin was shown to aid in the intracellular force balance of stretchable smooth muscle cells *in vitro* (Nagayama and Matsumoto, 2008). The meshwork of actin found within the constrictional epithelium may not only provide retention during stretching but also oppose the external forces produced by the tooth during the priming step. The constriction is thus likely to be a passive regulatory mechanism; it limits tooth movement until enough force is generated to bypass the constriction. By contrast, the proximal epithelium lacks the meshwork of microfilaments observed in the epithelium of the constriction. High-speed video observations show that the proximal epithelium compresses during the priming step (Fig. 5D), and thus microfilaments provide structural integrity to the constriction.

The combined data from morphological studies and high-speed videography suggest that a muscular sphincter located midway down the extended proboscis regulates pressurization and venom flow within the proboscis during prey capture (Figs 4 and 6). As in other

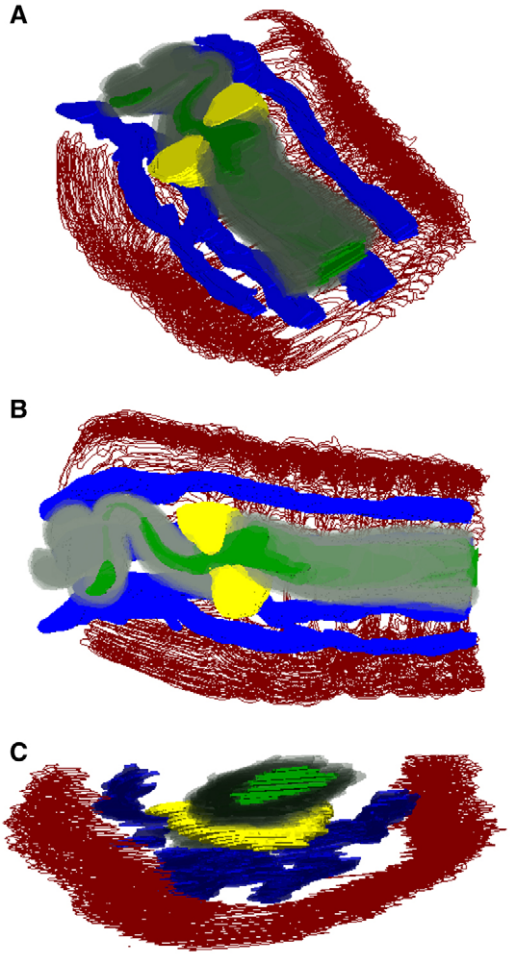

Fig. 6. Partial 3-D reconstruction of the circum-lumenal muscular sphincter in reference to the lumen wall and outer proboscis. The muscular sphincter (yellow) is shown to completely surround the lumen wall (gray). The lumen wall encloses the central cavity (green). Four distinct nerve bundles (blue) run longitudinally in this half of the proboscis surrounded by the outer proboscis wall (outlined in red). The models are oriented as follows: with the tip extending to right and out of the page (A), flat against the horizontal plane with the tip extending to the right (B), transverse orientation with the distal end in front (C). The curving of the lumen proximal to the muscular sphincter is an artifact caused by the excision process.

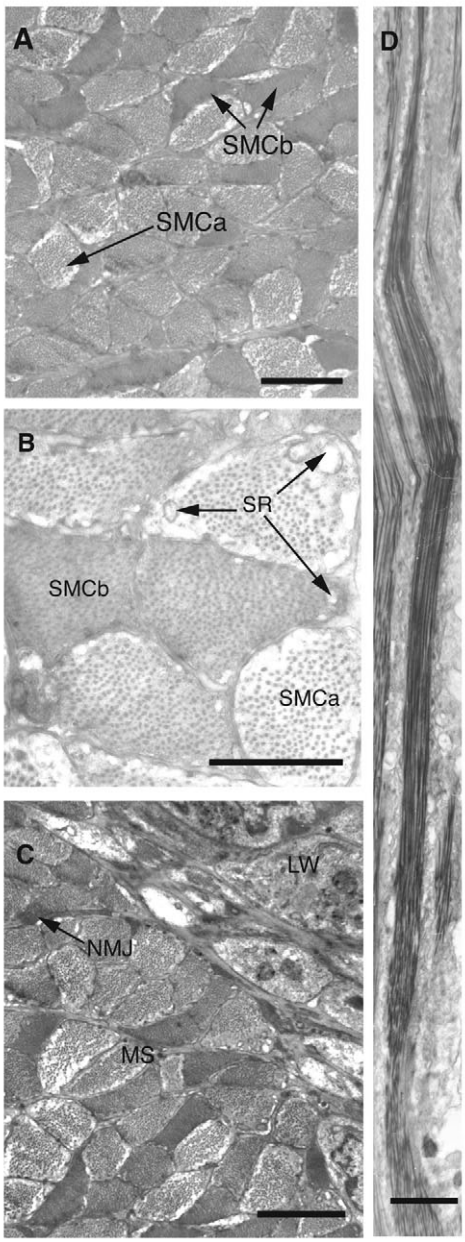

Fig. 7. Transmission electron micrographs (TEMs) of the muscle fibers inside the muscular sphincter. Low magnification view reveals the variation in muscle fibers labeled SMCa and SMCb (A). (B) Higher magnification of the different fiber types within the muscular sphincter. Innervation of the muscular sphincter adjacent to the lumen wall is shown (C). Photo-composite transverse section through the muscular sphincter (D). Scale bars in μm: A=5, B=2, C=5, D=5. LW, lumen wall; MS, muscular sphincter; NMJ, neuromuscular junction; SR, sarcoplasmic reticulum; SMC, smooth muscle cell.

muscular sphincters, flow within the proboscis lumen is likely to be regulated by contraction of the circular muscle fibers, which thereby constrict the lumen. The elongate cells that compose the muscular sphincter seem to lack the ultrastructure commonly seen in relatively rapidly contracting molluscan fibers, like the cross-striated muscles used in squid prey capture (Kier, 1985; Kier and Schachat, 2008). Nevertheless, the specialization of the muscular sphincter's fiber density and filament morphology, compared with the adjacent musculature, is adequate to regulate flow dynamics within the proboscis lumen. Relaxation of these muscle fibers within the sphincter allows venom to rapidly enter the proboscis lumen distal to the sphincter, suggesting that it may be pressurized upstream of the proboscis.

The sudden influx of venom into the distal proboscis lumen behind the base of the radular tooth causes the forward movement of the tooth observed during the priming step. While the tooth is forced against the constriction, pressure builds behind it, dilating the lumen. Observations of both *C. catus* and *C. pennaceus* show that lumen expansion peaks 2–3 ms prior to release of the tooth (Fig. 4D and supplementary material Fig. S3). This process may allow elastic energy to be stored in the lumen wall and released to accelerate the tooth past the constriction. Elastic energy storage in a hydraulic system such as this has been observed previously in the escape jet mechanism of the squid mantle (Macgillivray et al., 1999; Neumeister et al., 2000; O'Dor 1988; Thompson et al., 2002). This type of mechanism could provide a means of transiently storing the energy needed for both harpoon propulsion and venom injection through the tooth.

Prior to the firing of the tooth, the sudden increase in tortuosity proximal to the muscular sphincter (Fig. 5C) is likely to be caused by a rapid increase of pressure within the proboscis lumen. It is unlikely that the pressure increase is generated by the contraction of diffuse non-specialized smooth muscle surrounding the lumen in this portion of the proboscis (S.M.S., unpublished) and instead, more likely, by another mechanism elsewhere in the proximal proboscis or pharynx. The muscular sphincter may serve to limit the pressure and fluid flow to the distal proboscis. Indeed, during this stage of prey capture no forward movement of the radular tooth was observed, suggesting that the sphincter limits fluid release in the proboscis at least 108 ms prior to the appearance of venom in the lumen. Thus, the muscular sphincter may play a key role in regulating the biomechanics of prey capture within the proboscis. Additional research is needed on venom kinematics proximal to the proboscis, especially the dynamics of pressure change, fluid movement and the mechanisms of pressure generation.

Although the generation of pressure during *Conus* prey capture is not fully understood, it may share important features with holoplanktonic gastropods in the genus *Clione*. Prey capture in *Clione limacina* involves the rapid hydraulic inflation (50–70 ms) of buccal cones used to ensnare pelagic prey (Hermans and Satterlie, 1992). The pressure needed to inflate the buccal cones has been hypothesized to be generated by contraction of the musculature surrounding the hemocoelic fluid in the animal's head. Activation of the muscles in the head with the simultaneous activation of the buccal cone retractor muscles would cause an increase in hemocoelic pressure. The sudden relaxation of the retractor muscles would then result in the rapid inflation of the buccal cones (Norekian and Satterlie, 1993). Much in the same manner, simultaneous contraction of the muscular sphincter in the cone snail's proboscis and muscular elements proximal to the sphincter (such as in the pharynx) would generate an increase of pressure within the lumen. The timing needed to increase tortuosity of the proboscis lumen (~11 ms) suggests a rapid generation of pressure similar to that of *C. limacina*. Relaxation of the muscular sphincter would then result in the rapid release of venom into the lumen of the distal proboscis, propelling the radular tooth into prey.

Within a cone snail, a muscular bulb connects to a long tubular venom duct (the site of venom peptide synthesis) opposite from the duct's site of insertion into the pharynx (see Marshall et al., 2002). It is tempting to consider that the muscular bulb plays a central role in pressurization of the proximal proboscis lumen. However, as venom appears after pressurization and is subsequently flushed from the proboscis, the muscular bulb more likely plays a role in delivery of venom into the pharynx for expulsion by an as yet to be determined mechanism (such as contraction of the pharynx or contraction of musculature surrounding the visceral hemocoel, similar to *Clione*).

Results from our study suggest that venom is injected as a discrete volume into the prey of *C. pennaceus*. The concentration of venom within the lumen increases rapidly during the priming step, continues to increase as the radular tooth is propelled into prey and then decreases as it is flushed from the proboscis (Fig. 5A). As *C. pennaceus* often inject their prey multiple times by rapidly reloading the radular tooth within 2 min (S.M.S., unpublished), it may be important to control the volume of venom delivered per injection. This metering of venom expulsion is a common feature of venomous reptiles such as rattlesnakes (Young and Kardong, 2007) and invertebrates like the wandering spider, *Cupiennius salei* (Kuhn-Nentwig et al., 2004). By metering venom in this way and flushing it from the lumen, cone snails may reduce the amount of superfluous venom injected into prey. More studies are needed to elucidate the exact mechanism of the metering in *Conus*. Nevertheless, this transient pattern of flow may also protect against leakage of venom through the intermediate junctions of the epithelia into the hemocoel, an especially important feature for mollusc-hunting cones with venom components targeting molluscan physiology. A previous study suggested that venom is pre-loaded in the radular tooth (Marshall et al., 2002). Our data demonstrate, instead, that venom is dispensed rapidly as a discrete volume through the proboscis lumen and the radular tooth during prey capture.

Juvenile *C. pennaceus* are powerful models for understanding venom kinematics during prey capture. Previous research investigating venom kinematics focused primarily on snakes and lizards, in which the boney architecture of the head and obscure venom canals make visualization of venom difficult. Surgically implanted transonic flow probes have therefore been employed to analyze venom flow in snakes (Young et al., 2000; Young and Zahn, 2001) but the implanted device may alter the dynamics of flow. Although the proboscides of adult cone snails have pigmentation on the dorsal and ventral surfaces, the extended proboscis of a juvenile *C. pennaceus* is nearly transparent (Fig. 4). Additionally, the venom of mollusc-hunting cone snails contains opaque granules (Maguire and Kwan, 1992). Thus, one can observe both the dynamics of venom flow in the lumen and the role of important morphological elements during prey capture. To our knowledge, this is the first study to directly and non-invasively visualize venom kinematics during prey capture.

The evolution of venomous animals has been a subject of considerable interest to biologists. Strong correlations between the presence of a venom delivery system and diversification have been identified. For example, the advent of the ovipositional mechanism (used for venom injection) has been shown to be of primary importance for the evolution within Hymenoptera (Austin and Dowton, 1999). Other studies suggest that the evolution of venom was a key innovation driving the diversification of snakes and lizards (Fry et al., 2005). A diverse array of venom delivery mechanisms are observed in squamates. Venomous snakes have venom apparatus in the upper jaw, while lizards in the families Helodermatidae (Fry et al., 2005) and Varanidae (Fry et al., 2009) evolved a mandibular mode of envenomation. Further adaptation occurred within advanced snakes with front and rear fangs evolving in close association with a maxillary venom gland (Vonk et al., 2008). The presence of a venom gland allowed venomous vertebrates to independently evolve multiple effective modes of envenomation.

As in other venomous animals, rapid physiological and biomechanical venom delivery systems are needed in *Conus*. Following the evolution of a venom apparatus [venom duct and attached venom bulb (Taylor, 1990)], gastropods of the superfamily Conoidea (previously known as Toxoglossa) evolved a variety of feeding mechanisms (Kantor, 1990). Species in the genus *Conus* evolved a well-developed venom apparatus (Kantor, 1990), harpoon-like radular teeth (Kantor and Taylor, 2000; Kohn et al., 1999; Nishi and Kohn, 1999) and an intraembolic proboscis (Miller, 1989) with a muscular sphincter (Greene and Kohn, 1988). Our data suggest that all these features are prerequisites for the high-speed envenomation of prey seen in cone snails. Indeed, the presence of morphological features, including structures analogous to the muscular sphincter in cone snails, in the proboscides of other Conoidea superfamily members indicates that the development of a hydraulic mechanism antedates the genus (Kantor, 1990). In this context, high-speed hydraulic prey capture represents a key adaptation in the evolutionary and ecological radiation of Conoidea. The mechanism is a versatile method for injection of toxins, allowing these snails to expand the range of prey types exploited. Consequently, fish-hunters such as *C. catus* have not evolved hydraulic prey capture independently (Schulz

et al., 2004). In *Conus*, the evolution of an effective method to inject venom allows specialization of venom composition for specific prey types such as aquatic vertebrates (Duda and Palumbi, 2004). The rapid biomechanical injection mechanism and toxins thus represent key features in the diversification of the genus and its conspicuous presence in tropical marine habitats.

LIST OF ABBREVIATIONS

B	bulbous base of radular tooth
C	collagen
CE	constrictional epithelium
CM	circular musculature
CP	cytoplasm
DE	distal epithelium
f-actin	filamentous actin
H	hemocoel
L	ligament
LM	longitudinal musculature
LW	lumen wall
Mv	microvilli
MS	muscular sphincter
N	nucleus
NE	nerve
NMJ	neuromuscular junction
PE	proximal epithelium
PM	plasma membrane
PW	outer proboscis wall
R	ribbon-like microfilaments
S	shaft of radular tooth
SMC	smooth muscle cell
SR	sarcoplasmic reticulum
T	radular tooth
TEM	transmission electron microscopy
TW	terminal web
µf	microfilaments

ACKNOWLEDGEMENTS

We thank David M. James, Dr Jennifer A. Armstrong and Jennifer K. Phan for critical reading of an earlier version of this manuscript, Christine Pope Petersen for her initial sighting of venom movement in *C. pennaceus* and David M. James for additional tissue processing. We also thank Drs Renee Baran and Gretchen North for access to equipment. This work was supported by the Occidental College Undergraduate Research Center and a Fletcher Jones Research Fellowship to S.M.S.

REFERENCES

Austin, A. D. and Dowton, M. (1999). *Hymenoptera – Evolution, Biodiversity and Biological Control* (ed. A. Austin and M. Dowton), pp. 3. Collingwood, Victoria, Australia: CSIRO Publishing.

Davis, J., Jones, A. and Lewis, R. J. (2009). Remarkable inter- and intra-species complexity of conotoxins revealed by LC/MS. *Peptides* **30**, 1222-1227.

Duda, T. F. (2008). Differentiation of venoms of predatory marine gastropods: divergence of orthologous toxin genes of closely related Conus species with different dietary specializations. *J. Mol. Evol.* **67**, 315-321.

Duda, T. F. and Kohn, A. J. (2005). Species-level phylogeography and evolutionary history of the hyperdiverse marine gastropod genus Conus. *Mol. Phyl. Evol.* **34**, 257-272.

Duda, T. F. and Palumbi, S. R. (1999). Molecular genetics of ecological diversification: duplication and rapid evolution of toxin genes of the venomous gastropod *Conus*. *Proc. Natl. Acad. Sci. USA* **96**, 6820-6823.

Duda, T. F. and Palumbi, S. R. (2000). Evolutionary diversification of multi-gene families: allelic selection of toxins in predatory cone snails. *Mol. Biol. Evol.* **17**, 1286-1293.

Duda, T. F. and Palumbi, S. R. (2004). Gene expression and feeding ecology: evolution of piscivory in the venomous gastropod genus *Conus*. *Proc. R. Soc. Lond.* **271**, 1165-1174.

Duda, T. F., Kohn, A. J. and Palumbi, S. R. (2001). Origins of diverse feeding ecologies within Conus, a genus of venomous marine gastropods. *Biol. J. Linn. Soc.* **73**, 391-409.

Fiala, J. C. (2005). Reconstruct: a free editor for serial section microscopy. *J. Microsc.* **218**, 52-61.

Fry, B. G., Vidal, N., Norman, J. A., Vonk, F. F., Scheib, H., Ramjan, S. F. R., Kuruppu, S., Fung, K., Hedges, S. B., Richardson, M. K. et al. (2005). Early evolution of the venom system in lizards and snakes. *Nature* **439**, 584-588.

Fry, B. G., Wroe, S., Teeuwisse, W., van Osch, M. J. P., Moreno, K., Ingle, J., McHenry, C., Ferrar, T., Clausen, P., Scheib, H. et al. (2009). A central role for venom in predation by *Varanus komodoensis* (Komodo Dragon) and the extinct giant *Varanus* (*Megalania*) *priscus*. *Proc. Natl. Acad. Sci. USA* **106**, 8969-8974.

Greene, J. L. and Kohn, A. J. (1989). Functional morphology of the *Conus proboscis* (Mollusca: Gastropoda). *J. Zoo. Soc. Lond.* **219**, 487-493.

Hermans, C. O. and Satterlie, R. A. (1992). Fast-strike feeding behavior in a pteropod mollusk, *Clione limacine* Phipps. *Biol. Bull.* **182**, 1-7.

Huang, Z. and Satterlie, R. A. (1989). Smooth muscle fiber types and a novel patter on thick filaments in the wing of the pteropod mollusk *Clione limacine*. *Cell Tissue Res.* **257**, 405-414.

Jakubowski, J. A., Kelley, W. P., Sweedler, J. V., Gilly, W. F. and Schulz, J. R. (2005). Intraspecific variation of venom injected by fish-hunting Conus snails. *J. Exp. Biol.* **208**, 2873-2883.

Kantor, Y. (1990). Anatomical basis for the origin and evolution of the toxoglossan mode of feeding. *Malacologia* **32**, 3-18.

Kantor, Y. and Taylor, J. D. (2000). Formation of marginal radular teeth in Conoidea (Neogastropoda) and the evolution of the hypodermic envenomation mechanism. *J. Zoo. Soc. Lond.* **252**, 251-262.

Kier, W. M. (1985). The musculature of squid arms and tentacles: ultrastructural evidence for functional differences. *J. Morphol.* **185**, 223-239.

Kier, W. M. and Schachat, F. H. (2008). Muscle specialization in the squid motor system. *J. Exp. Biol.* **211**, 164-169.

Kohn, A. J. (1956). Piscivorous gastropods of the genus Conus. *Proc. Natl. Acad. Sci. USA* **42**, 168-171.

Kohn, A. J. (1990). Tempo and mode of evolution in Conidae. *Malacologia*. **32**, 55-67.

Kohn, A. J. and Hunter, C. (2001). The feeding process in *Conus imperialis*. *Veliger* **44**, 232-234.

Kohn, A. J., Nishi, M. and Pernet, B. (1999). Snail spear and Schimitars: a character analysis of Conus radular teeth. *J. Mollus. Stud.* **65**, 461-481.

Kuhn-Nentwig, L., Schaller, J. and Nentwig, W. (2004). Biochemistry, toxicology and ecology of the venom of the spider *Cuppiennius salei* (Ctenidae). *Toxicon.* **43**, 543-553.

Macgillivray, P., Anderson, E., Wright, G. and Demont, M. E. (1999). Structure and mechanics of the squid mantle. *J. Exp. Biol.* **202**, 683-695.

Maguire, D. and Kwan, J. (1992). *Coneshell venoms-synthesis and packaging. Toxins and Targets* (ed. D. Watters, M. Lavin and J. Pearn), pp. 11-18. Newark, NJ, USA: Harwood Academic Publishers.

Marshall, J., Kelley, W. P., Rubakhin, S. S., Bingham, J.-P., Sweedler, J. V. and Gilly, W. F. (2002). Anatomical correlates of venom production in *Conus californicus*. *Biol. Bull.* **203**, 27-41.

Martin, G. G. and Talbot, P. (1981). The role of follicular smooth muscle cells in hamster ovulation. *J. Exp. Zool.* **216**, 469-482.

Miller, J. A. (1989). The toxoglossan proboscis structure and function. *J. Moll. Stud.* **55**, 167-181.

Nagayama, K. and Matsumoto, T. (2008). Contribution of actin filaments and microtubules to quasi-in situ properties and internal force balance of cultured smooth muscle cells on a substrate. *Am. J. Cell Physiol.* **295**, 1569-1578.

Neumeister, H., Ripley, B., Preuss, T. and Gilly, W. F. (2000). Effects of temperature on escape jetting in the squid *Loligo opalescens*. *J. Exp. Biol.* **203**, 547-557.

Nishi, M. and Kohn, A. J. (1999). Radular teeth of Indo-Pacific molluscivorous species of Conus: a comparative analysis. *J. Mollus. Stud.* **65**, 483-497.

Norekian, T. P. and Satterlie, R. A. (1993). Co-activation of antagonistic motoneurons as a mechanism of high-speed hydraulic inflation of prey capture appendages in the pteropod mollusk, *Clione limacine*. *Biol. Bull.* **185**, 240-247.

O'Dor, R. K. (1988). The forces acting on swimming squid. *J. Exp. Biol.* **203**, 421-442.

Olivera, B. M. (1997). Conus venom peptides, receptors and ion channel targets, and drug design-50 million years of neuropharmacology. *Mol. Biol. Cell* **8**, 2101-2109.

Olivera, B. M. (2001). Conotoxins, in retrospect. *Toxicon.* **39**, 7-14.

Olivera, B. M. (2006). Conus peptides: biodiversity-based discovery and exogenomics. *J. Biol. Chem.* **281**, 31173-31177.

Plesch, B. (1977). An ultrastructural study of the musculature of the pond snail *Lymnaea stagnalis* (L.). *Cell Tissue Res.* **180**, 317-340.

Remigio, E. A. and Duda, T. F. (2008). Evolution of ecological specialization and venom of a predatory marine gastropod. *Mol. Ecol.* **17**, 1156-1162.

Schulz, J. R., Norton, A. G. and Gilly, W. F. (2004). The projectile tooth of a fish-hunting cone snail: *Conus catus* injects venom into fish prey using a high-speed ballistic mechanism. *Biol. Bull.* **207**, 77-79.

Spurr, A. (1969). A low viscosity epoxy embedding medium for electron microscopy. *J. Ultrastruct. Res.* **26**, 31-43.

Stewart, J. and Gilly, W. F. (2005). Piscivorous behavior of a temperate cone snail, *Conus californicus*. *Biol. Bull.* **209**, 146-153.

Taylor, J. (1990). The anatomy of the foregut and relationships in the Terebridae. *Malacologia* **32**, 19-34.

Thompson, J. T. and Kier, W. M. (2002). Ontogeny of squid mantle function: changes in the mechanics of escape-jet locomotion in the oval squid, *Sepioteuthis lessoniana*, Lesson, 1830. *Biol. Bull.* **203**, 14-26.

Vonk, F. J., Admiraal, J. F., Jackson, K., Reshef, R., de Bakker, M. A. G., Vanderschoot, K., van den Berge, I., van Atten, M., Burgerhout, E., Beck, A. et al. (2008). Evolutionary origin and development of snake fangs. *Nature* **454**, 630-633.

Wollensen, T., Wanninger, A. and Klussmann-Kolb, A. (2007). Myogenesis in *Aplysia californica* (Cooper, 1863) (Mollusca, Gastropoda, Opisthobranchia) with special focus on muscular remodeling during metamorphosis. *J. Morphol.* **269**, 776-789.

Young, B. A. and Kardong, K. V. (2007). Mechanisms controlling venom expulsion in the western diamondback rattlesnake, *Crotalus atrox*. *J. Exp. Zool.* **307**, 18-27.

Young, B. A. and Zahn, K. (2001). Venom flow in rattlesnakes: mechanics and metering. *J. Exp. Biol.* **204**, 4345-4351.

Young, B. A., Zahn, K., Blair, M. and Lalor, J. (2000). Functional subdivision of the venom gland musculature and the regulation of venom expulsion in rattlesnakes. *J. Morphol.* **246**, 249-259.

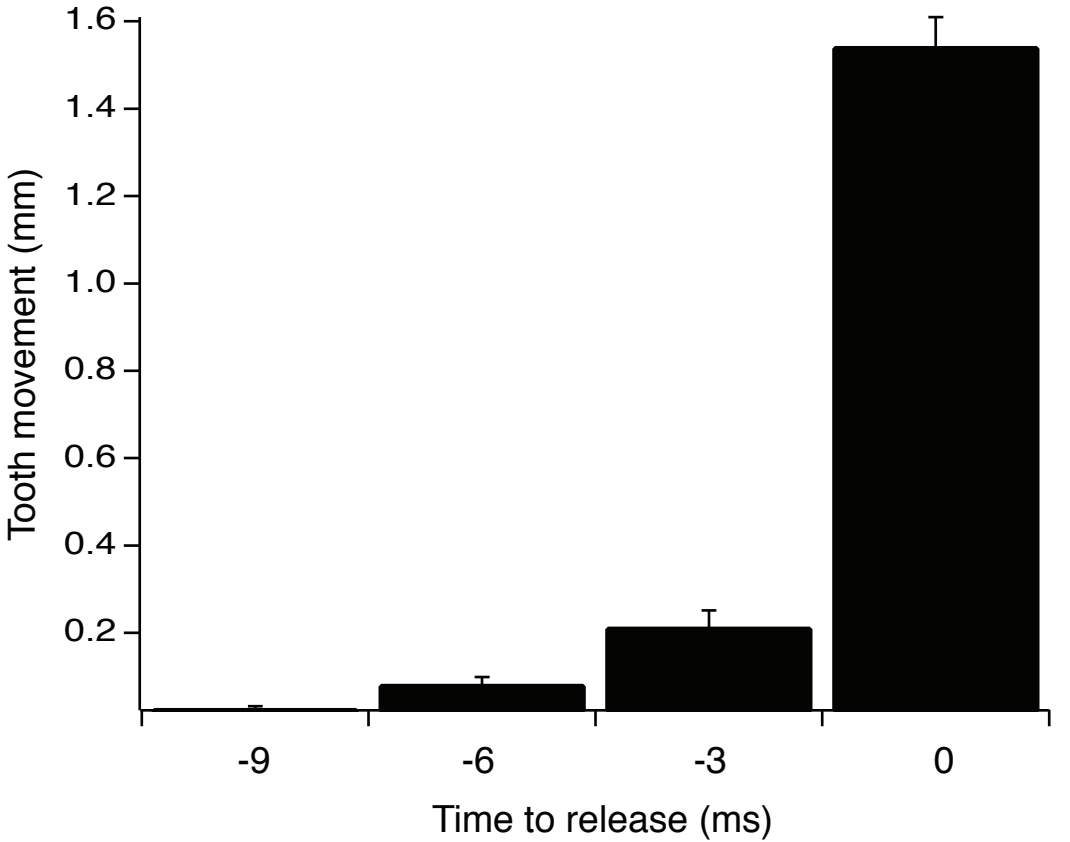
1.6
1.4
1.2
1.0
0.8
0.6
0.4
0.2
Tooth movement (mm)
-9
-6
-3
0
Time to release (ms)

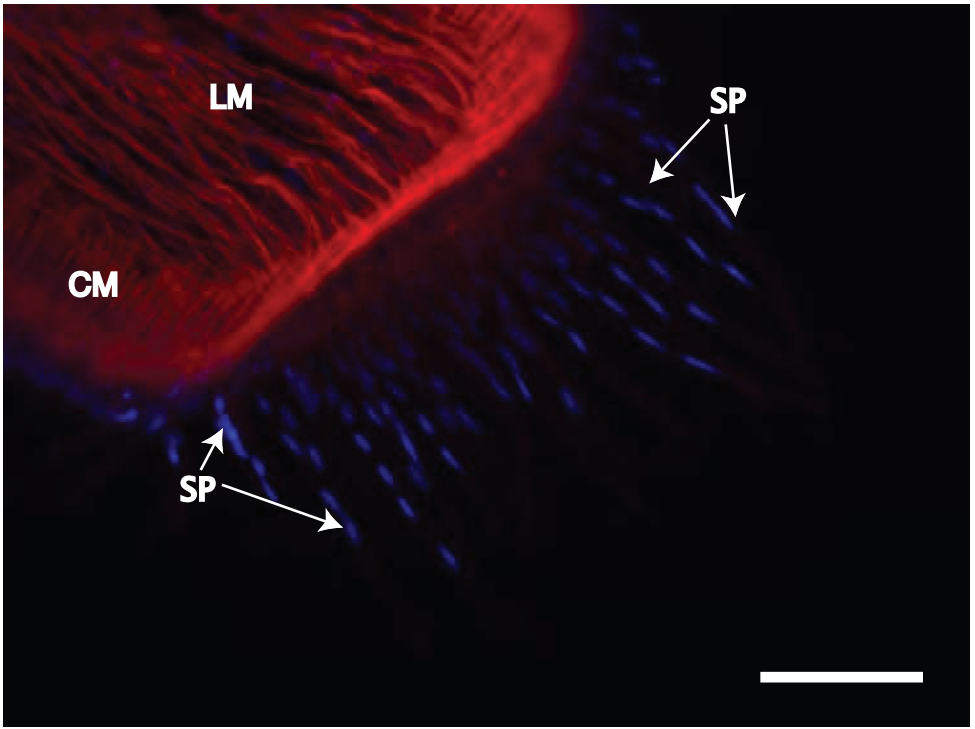
LM
SP
CM
SP

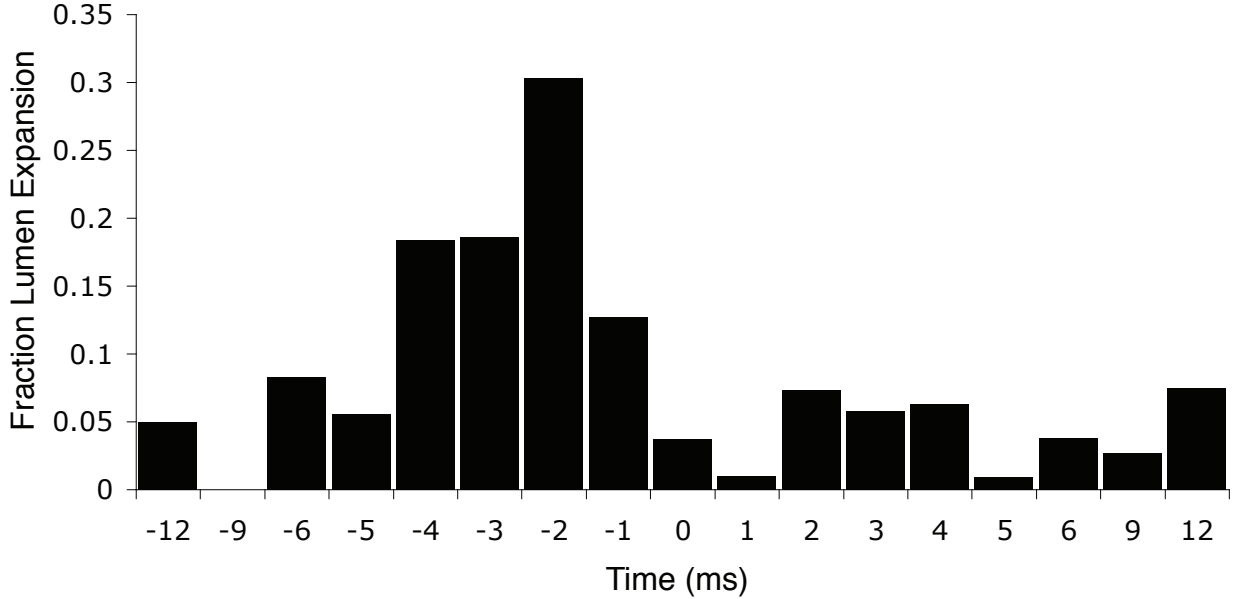
Fraction Lumen Expansion
0.35
0.3
0.25
0.2
0.15
0.1
0.05
0
-12
-9
-6
-5
-4
-3
-2
-1
0
1
2
3
4
5
6
9
12
Time (ms)

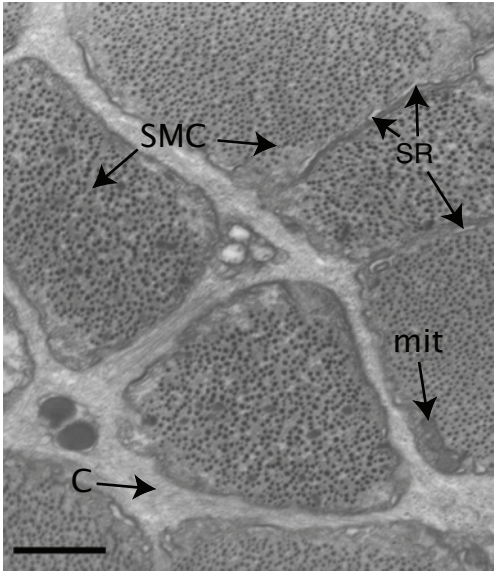
SMC
SR
mit
C

Table S1. Comparison between longitudinal musculature and two different smooth muscle cell (SMCs) types found in the muscular sphincter

	Cross-sectional size of fiber (μm)	Diameter of thick filament (nm)	Density of thick filaments in 1 μm^2
Longitudinal	2.2±0.6	44±0.6	92±6.9
SMCa	8.9±1.7	64±8.0	44.6±1.4
SMCb	5.7±1.5	43±0.9	85±5.6

Pairwise Student's *t*-tests reveal that all SMCs examined had statistically significant differences in fiber diameter ($P<0.05$). SMCa has a statistically significant difference in thick filament diameter as well as a decreased filament density ($P<0.05$). All other values were not significant ($P>0.05$).